Environmental Science and Pollution Research (2021) 28:39637–39647
https://doi.org/10.1007/s11356-021-13532-2

RESEARCH ARTICLE

Novel organic assisted Ag-ZnO photocatalyst for atenolol and acetaminophen photocatalytic degradation under visible radiation: performance and reaction mechanism

Bhuvaneswari Ramasamy[1] · Jeyanthi Jeyadharmarajan[1] · Prakash Chinnaiyan[2]

Received: 9 November 2020 / Accepted: 15 March 2021 / Published online: 24 March 2021

Abstract

This study is on photocatalytic degradation of pharmaceutical residues of atenolol (ATL) and acetaminophen (ACT) present in secondary effluent under visible light irradiation stimulated by Ag doped ZnO (Ag-ZnO) photocatalyst. *Lawsonia inermis* leaf extract was used for reduction of Zinc sulphate to ZnO nanoparticles (NPs). Further, ZnO NPs were doped with Ag and characterized by XRD, FT-IR, SEM-EDX, surface area analyzer, UV-Vis, and photoluminescence spectrometry to analyze the structure, morphology, chemical composition, and optical property. FT-IR analysis revealed major functional groups such as OH, C=O, and SEM analysis depicted the polyhedron shape of the NPs with size range of 100 nm. Ag-ZnO NPs were used in the photocatalytic degradation of ATL and ACT, and its removal was evaluated by varying initial contaminant concentration, catalyst dosage, and initial pH. Findings indicate that Ag-ZnO NPs demonstrated relative narrow bandgap and efficient charge separation that resulted in enhanced photocatalytic activity under visible light illumination. The photocatalytic degradation of ATL and ACT fitted well with pseudo-first-order kinetic model. Further, it was found that under optimal conditions of 5 mg/L of contaminants, pH of 8.5, and catalyst dose of 1 g/L, degradation efficiency of 70.2% (ATL) and 90.8% (ACT) was achieved for a reaction time of 120 min. More than 60% reduction in TOC was observed for both contaminants and OH• pathway was found to be the major removal process. Ag-ZnO photocatalyst showed good recycling performance, and these findings indicate that it could be cost effectively employed for removing emerging contaminants under visible light radiation.

Keywords Organic synthesis · Photocatalysis · *Lawsonia inermis* (Henna) · Wastewater treatment · Pharmaceutical contaminants

Introduction

India is the largest producer and exporter of generic drugs, and in this COVID-19 pandemic condition, it is strengthening its pharmaceutical production capacity and is a strong contender for mass production of future COVID-19 vaccination. But this huge production of drugs leads to the exploitation of natural water sources as untreated or partially treated wastewaters from pharmaceutical industries are discharged into surface and groundwater (Ankush et al. 2018; Larsson 2014). Pharmaceutical occurrence review studies have reported the occurrence of pharmaceuticals in wastewater effluents, surface, and groundwater sources globally (Patel et al. 2019) and in India (Balakrishna et al. 2017). Though the natural degradation processes and the various wastewater treatment process remove the API to some extent, majority of parent compounds and its metabolites are not removed in the conventional wastewater treatment plant (WWTP) which could cause acute and chronic toxicity to various organisms including human beings (Freitas et al. 2017; Schröder et al. 2016; Aus der Beek et al. 2016; Grenni et al. 2018). Among the various pharmaceutical contaminants (PCs), ATL and ACT which are critical compound for Indian environment are considered in this study (Chinnaiyan et al. 2018). ATL belongs to beta blocker group drug often used to treat high blood pressure, migraine headache,

Responsible Editor: Sami Rtimi

✉ Jeyanthi Jeyadharmarajan
j.jeyanthigct@gmail.com

[1] Department of Civil Engineering, Government College of Technology, Coimbatore, Tamilnadu 641013, India

[2] Department of Civil Engineering, Amrita Vishwa Vidyapeetham, Coimbatore, India

and heart-related pains. ACT is classified under analgesic drug class which is a commonly prescribed pain killer. Previous studies were reported about the occurrence of ATL and ACT in WWTP effluents and water bodies worldwide and suggested the need for adopting advanced treatment options (Khan et al. 2020; Tran et al. 2018).

Heterogeneous photocatalysis is a promising technology and can efficiently remove most of the emerging contaminants and can be conveniently employed as tertiary treatment process in the existing WWTPs (Moles et al. 2020, Chinnaiyan et al. 2019). ZnO is one of widely used photocatalysts owing to its high exciton-binding energy (~60 meV), wide bandgap energy (~3.37 eV), availability at low cost, and high oxidative ability. But the wide bandgap energy imposes limitation of its usage as visible light-induced photocatalyst, and also, its photocatalytic efficiency is restricted due to swift recombination rate of electron-hole pairs. These limitations can be improved by various approaches such as doping, co-doping, and fabricating composites (Mohd et al. 2016, Akir et al. 2017). Doping of ZnO with noble metals such as Si, Cu, Pd, Ag, and Au has shown improvement in its charge separation and visible light optical absorption. Among these metals, silver has gained importance by showing strong absorption of visible light and inhibition of electron-hole recombination through surface plasmon resonance (Kaur et al. 2018).

There are several studies reporting various synthesis procedures to produce Ag-ZnO nanoparticles such as hydrothermal synthesis, sol-gel method, and coprecipitation. The drawback in the chemical route of synthesis involves release of harmful byproducts arising from toxic reducing agents, contamination of precursors, and undesired detrimental impacts on the environment. To overcome these limitations, there are studies utilize plants or microorganisms as reducing and capping agent in the synthesis of NPs. Recently, there are several studies report synthesis of ZnO NPs from neem leaves (Elumalai and Velmurugan 2015), aloe vera (Ali et al. 2016), and sandal wood leaves (Kavithaa et al. 2016).

In the present work, the Ag-ZnO photocatalyst was synthesized, and characterization was performed to evaluate their morphology, structure, crystalline phase, surface area, and optical properties. The characterization techniques include XRD, FT-IR, SEM-EDX, surface area analysis, UV-visible, and photoluminescence spectrometry. The efficiency of Ag-ZnO as a photocatalyst in the visible region was evaluated by the degradation of two PCs, viz., ATL and ACT which were spiked in the treated domestic wastewater effluent. The four parameters that were considered in this study include initial contaminant concentration, initial pH, catalyst dosage, and reaction time, and the degradation of PCs was investigated. PC degradation kinetic studies and photocatalyst recycling performance analysis were also examined.

Materials and methods

Material

ATL and ACT of purity 99%, zinc sulphate ($ZnSO_4$), and silver nitrate ($AgNO_3$) were received from Sigma-Aldrich and used as received. Chemical structure and properties are presented in Table 1 and Fig. 1. Hydrochloric acid and sodium hydroxide were purchased from Merck. All other chemicals used in this study were of analytical grade, and all solutions were prepared using deionized water obtained from Milli-Q water purification system. *Lawsonia inermis* leaves were collected and washed before using it for further process.

Synthesis of Ag-ZnO photocatalyst

Lawsonia inermis leaves were collected and washed several times in running tap water and distilled water and sun dried to remove residual moisture. Fifty grams of these leaves was added with 100 ml of deionized water and boiled for 60 min to obtain the leaf extract. The extract was cooled and filtered using Whatman Filter Paper No. 1, and the filtered extract was then stored at room temperature. The functional groups present in the leaf extract (Fig. 3) served as reducing agent which could reduce Zn^{2+} to Zn^{+} ions and finally to zinc nanoparticles. Ten milliliters of this leaf extract was boiled, and when temperature reached 60°C, 1g of zinc sulphate was added and this solution was boiled till it turned into paste. This paste was dried at 80°C for 24 h and calcined at 450°C for 2 h to obtain zinc oxide nanoparticles. 0.01M solution of silver nitrate was added drop by drop to as-prepared zinc oxide nanoparticle under constant stirring, to obtain slurry form. This slurry was washed using deionized water and was dried at 80°C for 24 h and calcined at 300°C for 2 h. The resultant Ag-ZnO was used as photocatalyst in this study. Simultaneously, a blank sample with only the zinc sulphate solution without the plant extract was also maintained at a similar experimental condition. Production of nanoparticles was not observed in the blank sample.

Table 1 Properties of atenolol and acetaminophen

Property	Atenolol	Acetaminophen
Therapeutic group	Beta blocker	Analgesics and antipyretics
Molecular formula	$C_{14}H_{22}N_2O_3$	$C_8H_9NO_2$
Molecular weight	266.3 g/mol	151.16 g/mol
Log K_{ow}	0.16	0.46
pK_a	9.6	9.38

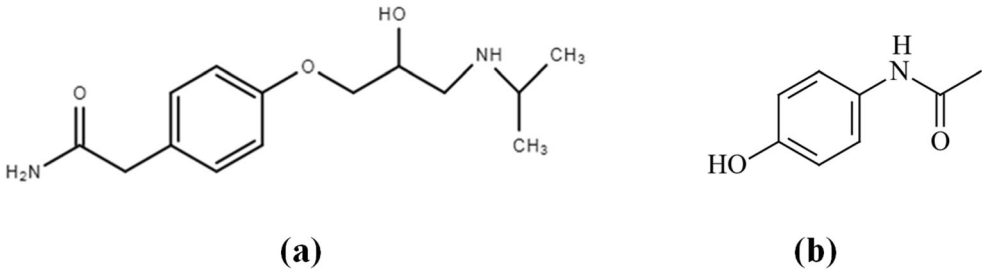

(a) (b)

Fig. 1 Chemical structure of **a** atenolol and **b** acetaminophen

Characterization techniques

Phase identification of Ag-ZnO was carried out by employing X-ray diffractometer PANALYTICAL model X'Pert^3 powder diffractometer with $Cu_{K\alpha}$ radiation (λ = 1.5406 Å). Diffraction studies were conducted in the 2θ scale between 30° and 80°. Fourier transform infrared (FTIR) spectra were collected using Perkin Elmer spectrum two FTIR spectrophotometer in the range of 4000–400 cm^{-1} to identify the functional groups present in the synthesized nanocatalyst. Morphology as well as particle size of the as-prepared photocatalyst was examined using SIGMA HV-CARL ZEISS field emission scanning electron microscope (FESEM) at an accelerating voltage of 10 kV and energy dispersive X-ray (EDX). In addition, the Brunauer-Emmett-Teller (BET) surface area characteristics were measured by surface area analyzer (BELSORP mini II). The ultraviolet-visible absorption studies of the photocatalyst were conducted on an UV-Vis spectrophotometer (PerkinElmer Lambda 35) which is having continuous scan mode of scan range 200–700 nm and scan speed of 480 nm with slit width of 1nm. Room temperature photoluminescence spectra of the photocatalyst were collected from Perkin-Elmer LS45 spectrometer using xenon flash lamp laser as the excitation source within the range of 300 to 500 nm and excitation wavelength of 325 nm.

Photocatalytic activity evaluation

Photocatalytic activity of Ag-ZnO was evaluated by measuring the degradation of ATL and ACT in aqueous solution. Standard stock solution was prepared by dissolving 0.25 g of ATL and ACT in 500 mL deionized water. From this standard stock solution, working solutions ranging from 5 to 20 mg/L were prepared following dilutions. To access the performance of photocatalyst, the APIs were spiked in the treated effluent (Table S1 supplementary material: characteristics of secondary effluent) collected from WWTP at Coimbatore, India, and the performance was recorded. Photocatalytic analysis was carried out using visible light photo reactor (Fig. S1) consists of borosilicate immersion jacketed tube to hold the 300W Tungsten halogen lamp with inlet and outlet for water circulation to cool the lamp surrounded by sample tubes. In a typical experiment, diluted solution containing pharmaceutical contaminants was mixed with measured quantity of photocatalyst and initial pH was adjusted using hydrochloric acid (HCl) and sodium hydroxide (NaOH). This solution was under constant stirring for a period of 30 min to attain absorption desorption equilibrium between substrate and catalyst. After this, the suspension was irradiated in visible reactor for specified period of time. At regular time interval, samples were withdrawn, subjected to centrifugation (SIGMA, 2-16KL) for 15 min at 1000 rpm for the separation of catalyst particles which were filtered using 0.45μm filters, and the filtrate was taken for further analysis. The ATL and ACT concentrations were analyzed using HPLC (Shimadzu LC-2010CHT) at an absorbance of 225 nm and 264 nm, respectively. The mobile phase consisted of methanol and deionized water mixture in the ratio 70:30 (v/v). All experiments were conducted in triplicate, and mean value was reported. The percent removal of contaminant was calculated using Eq. (1).

$$\text{Contaminant removal}\ (\%) = \frac{C_o - C}{C_o} \times 100, \tag{1}$$

where C_o is the initial contaminant concentration and C is the final contaminant concentration after treatment.

The main reactive species responsible for degradation of ATL and ACT was investigated further by conducting separate set of characteristic experiments and analyzing the photocatalytic process.

Kinetic studies

The kinetics of ATL and ACT photocatalytic degradation rate and mineralization was analyzed using pseudo-first-order reaction model (Eq. (2)).

$$-\frac{dC}{dt} = k_{\text{obs}} C. \tag{2}$$

Equation (2) can be rewritten as

$$\ln\left(\frac{C}{C_o}\right) = -k_{\text{obs}} t, \tag{3}$$

where k_{obs} is the pseudo-first-order degradation rate constant (min^{-1}).

$$r_{\text{obs}} = -k_{\text{obs}} C_o. \tag{4}$$

The pseudo-first-order rate of ATL and ACT photocatalytic degradation was calculated from Eq. (4).

Results and discussion

Morphology and crystal structure

X-ray diffraction patterns of pure ZnO and Ag-ZnO are presented in Figs. 2a, b, respectively. Analyzing the XRD pattern of pure ZnO, it can be attributed to hexagonal wurtzite structure of ZnO without phase modifications and impurities. The peak positions are in good agreement with JCPDS file No. 36-1451. The diffraction peaks of single-phase ZnO are exhibiting superior quality crystalline characteristics which can be attributed to strong and sharp peaks. Analyzing the XRD pattern of Ag-ZnO, additional peaks (marked with symbol #) other than that of pure ZnO are observed which is due to the result of doping of ZnO with Ag ions. The diffraction peaks of (111), (200), and (220) represent crystal planes of face-centered metallic Ag in agreement with JCPDS file No. 04-0783 (Liu et al. 2018).

The development of nanocrystalline ZnO wurtzite configuration and the outcome of silver addition were confirmed by FT-IR spectral studies. The IR spectra of *Lawsonia inermis* leaf extract, pure ZnO, and Ag-ZnO are presented in Fig. 3. As discussed earlier, the leaves of *Lawsonia inermis* were acting as reducing agent and it contain various chemical elements such as lawsone, flavonoids, and tannin which aided in formation of ZnO nanoparticles. The Henna leaf extract consists of lawsone (2-hydroxy-1,4-naphthaquinone) as its main constituents that contain p-benzoquinone unit, benzene unit, and phenolic group. Also, it contains flavonoids and coumarins. Hydroxyl (OH) and carbonyl (C=O) groups are the two major frequency regions denoting the presence of lawsone and tannin of *Lawsonia inermis* (Zulkifli et al. 2017). The broad absorption peak from 3200 to 3450 cm^{-1} indicates O-H stretch corresponding to alcoholic hydraulic group. The band at 1362 cm^{-1} indicates the presence of C-O-H bending mode (Sundrarajan et al. 2015). The stretching vibration

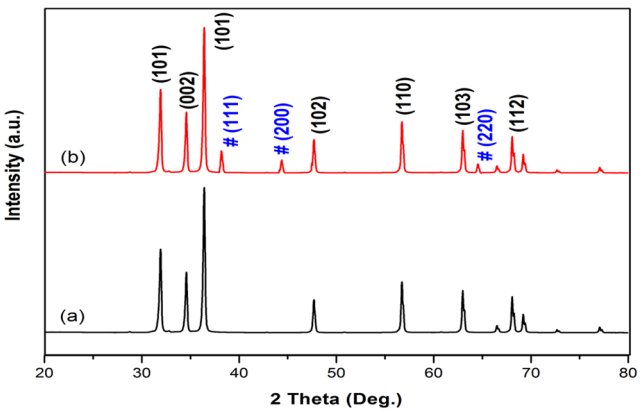

Fig. 2 XRD pattern of **a** pure ZnO and **b** Ag-ZnO

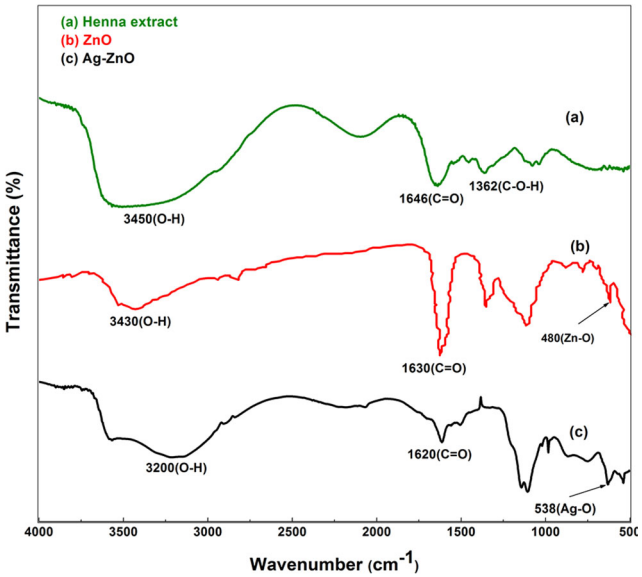

Fig. 3 FTIR spectrum of **a** Henna leaf extract, **b** pure ZnO, and **c** Ag-ZnO

of carbonyl group characteristic of the secondary amides and other compounds containing C=O group gave rise to band around 1640 cm^{-1} (Yadav et al. 2018, Sajan et al. 2017). Strong spectral peak at 3430 cm^{-1} in Fig. 3b indicates the presence of O-H bond which eventually denotes the availability of adequate amount of hydroxyl groups on surface of prepared ZnO (Zare et al. 2019). Also, the stretching frequency at 480 cm^{-1} denotes the ZnO bond (Fig. 3b) which had emerged as weak bond in Fig. 3c with addition of Ag.

Observing the spectra of Ag-ZnO, slight change in peak and their intensities can be noted in comparison to pure ZnO. This could be ascribed to interaction of Ag with ZnO nanoparticles in the formation of Ag-ZnO NPs. The hydroxyl groups were notably shifted to 3200 cm^{-1}. Also, spectral peak at 538 cm^{-1} can be attributed to characteristic stretching mode of Ag-O (Sajan et al. 2017).

SEM analysis (Fig. 4) revealed the presence of rod and spherical shaped nanoparticles in the size range of 100 nm, and it also revealed the presence of Ag NPs which are dispersed in ZnO NPs. The corresponding EDX spectrometer pattern was evaluated (Fig. 5) which confirms the presence of Zn, O, and Ag elements with weight percentage of 10.6, 41.4, and 4.6, respectively. The weight percentage of Ag was found matching with the actual metal addition in the synthesis process. In addition to the above elements, C was the only major impurity observed which possibly could have occurred due to the green synthesis process.

Surface area characteristics

The BET surface area and pore structure of the Ag-ZnO were investigated by the Brunauer-Emmett-Teller N_2 adsorption-desorption isotherms at adsorption temperature of 77 K (Fig. 6). The adsorption-desorption isotherm of Ag-ZnO confirms

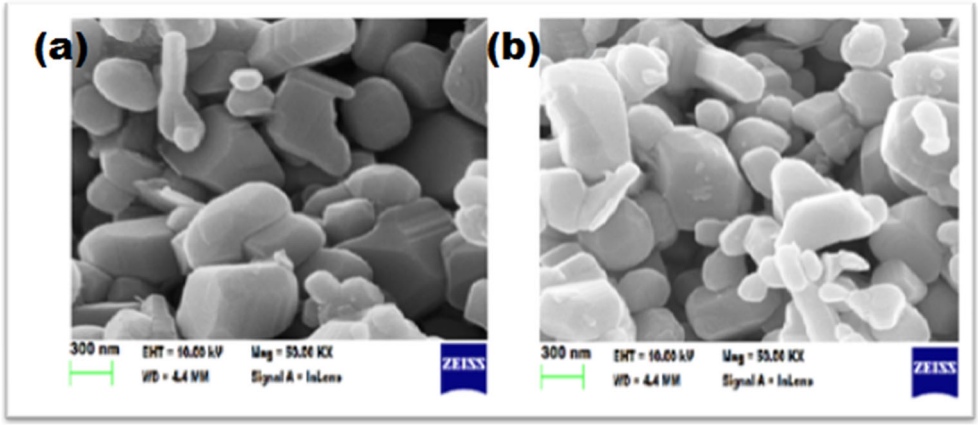

Fig. 4 SEM images of **a** pure ZnO and **b** Ag-ZnO

the type IV isotherm because of formation of hysteresis loop conforming to IUPAC classification of mesoporous materials (Kadam et al. 2018). From the nitrogen desorption, BJH mesopore sizes were obtained and pore volumes were determined from cumulative volume of pores. The ZnO nanoparticle had a surface area, pore volume, and pore diameter of 7.58 m^2/g, 0.06 cm^3/g, and 32.56 nm, respectively, while the corresponding values of Ag-ZnO were found to be 35.3 m^2/g, 0.082 cm^3/g, and 26.57 nm, respectively. An increase of 365% in the surface area, 36.6% rise in pore volume, and 18.4% reduction in pore diameter for Ag-ZnO were observed in comparison to ZnO indicating that all these parameters were improved due to the addition of Ag with ZnO. Literature confirms that the higher specific surface area is the photocatalytic activity resulting in improved performance of Ag-ZnO as a photocatalyst in comparison to ZnO.

Influence of Ag-ZnO on optical absorption

The UV-visible absorption spectra of ZnO and Ag-ZnO samples are presented in Fig. 7. The sharp peak at 357 nm in ZnO is the result of absorption in pure ZnO due to exciton formation. Assynthesized Ag-ZnO improved the absorption in the visible region of wavelength range 400–500 nm towards red shift due to localized surface plasmon–exciton coupling. This could be possible from low intrinsic losses of Ag NPs which causes narrow SP resonances with prominent optical field augmentation (Achermann 2010). Also, transfer of electrons from higher fermi energy (Ag) state to lower fermi energy (ZnO) results in spectra shift towards visible light region. The bandgap energy values of pure ZnO and Ag-ZnO calculated from UV-Vis absorption spectra were 3.31 eV and 3.02 eV, respectively. The red shift signifies that bandgap energy of Ag-ZnO is less than that of pure ZnO.

In order to quantify the structural defects and energy bands in materials, photoluminescence spectra of ZnO and Ag-ZnO were recorded at an excitation wavelength of 325 nm and are presented in Fig. 8. PL spectra can be able to provide information about the recombination of photoinduced electrons and holes, and low PL intensity indicates low recombination rate. PL spectra were showing strong UV emission peak centered at 393 nm which could be assigned to the near band edge emission of ZnO. The peaks at 461 and 547 nm could have

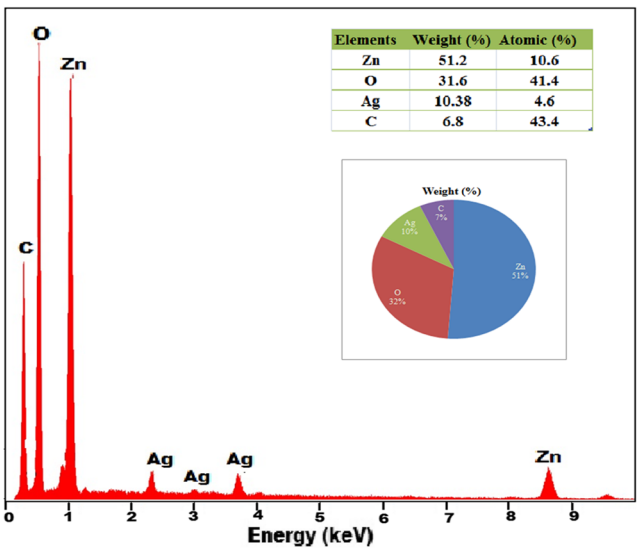

Fig. 5 SEM EDX spectra of Ag-ZnO

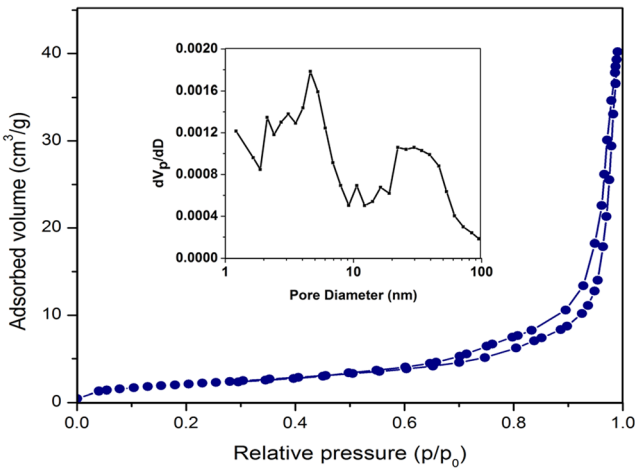

Fig. 6 BET surface area nitrogen adsorption-desorption isotherm of Ag-ZnO. Inset is the distribution of pore diameter

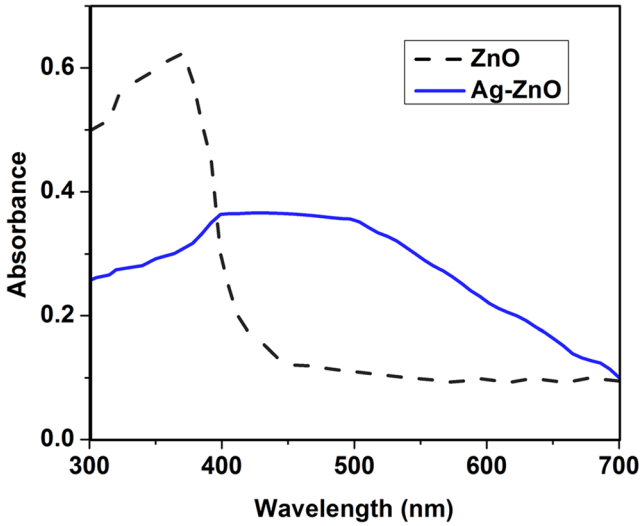

Fig. 7 UV-Vis absorption spectra of ZnO and Ag-ZnO

been resulted from bound excitons and structural defects on ZnO surface. Also, the PL spectra of Ag-ZnO show a decrease in emission intensity which positively correlates with low electron-hole recombination rate which eventually increases the lifespan of photo-generated charge carriers. The results obtained from optical studies show the improvement in the visible light absorption and subsequent enhancement in visible light photocatalytic activity resulting from incorporation of Ag into ZnO.

Photocatalytic degradation of ATL and ACT

The as-synthesized Ag-ZnO was used as photocatalyst, and degradation studies of ATL and ACT were performed.

Effect of initial contaminant concentration

To evaluate the effect of initial ATL and ACT concentration, in the photocatalytic degradation process, experiments were carried out by varying the contaminant concentration in the range of 5–20 mg/L with Ag-ZnO loading of 1 g/L, and the results are presented in Fig. 9. The logarithmic plot of contaminant concentration against irradiation time (inset of Fig. 9) confirms that degradation of ATL and ACT follows the pseudo-first-order kinetics, and the rate constants are presented in Table 2. The k_{obs} decreased from 0.01 to 0.008 min^{-1} when initial ATL concentration ($[ATL]_{int}$) increased from 5 to 20 mg/L. Increase in $[ACT]_{int}$ also exhibited the same decreasing trend (from 0.02 to 0.009 min^{-1}). This could be explained that at higher concentrations, more active sites of Ag-ZnO could be occupied by contaminants, and as a result, the generation of oxidants could be hindered. There is ample possibility for reaction intermediates formed in due course to occupy the active sites and also intercept the photons generated by visible light. Therefore, insufficient availability of OH• leads to a decrease in degradation of ATL and ACT at higher concentrations. Similar observations were reported in earlier studies involving OH• and visible light irradiance.

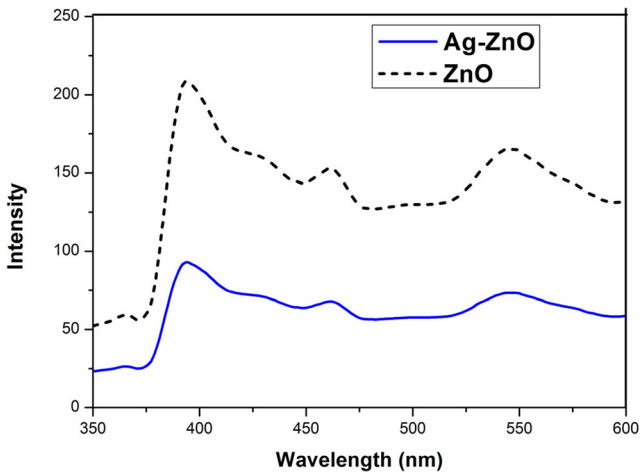

Fig. 8 PL spectra of ZnO and Ag-ZnO

Effect of pH

Most metal oxides including ZnO show amphoteric behavior due to which it can influence the surface reactions taking place on the catalyst surfaces. Since the pH of wastewater effluent may not be neutral and photocatalytic process is controlled by pH, the influence of pH on the rate of degradation of ATL and ACT was analyzed. The pH value of solution was varied from 4 to 12, and the variation of rate constants is presented in Fig. 10. The degradation rate of both contaminants increases as the pH increase from 4 to 8.5. With further increase in pH, a reduction in rate constant was observed. Maximum rate constant of 0.01 min^{-1} for ATL (corresponding to 70.2% removal) and 0.02 min^{-1} for ACT (90.8%) was observed at pH of 8.5.

This can be explained using electrostatic forces between the contaminants and catalyst. At pH values more than point of zero charge (pH_{zpc}), catalyst surface is negatively charged and vice versa. From literature, the pH_{zpc} of Ag-ZnO has the same pH_{zpc} of ZnO which is equal to 9.0 (Sushma and Girish Kumar 2017). The acid-ionization constant (pKa) of ATL and ACT is 9.6 and 9.5, respectively. Hence, increase in pH (> 9) steadily accelerates the electrostatic repulsion between Ag-ZnO surface and contaminants which negatively influence the mineralization and thereby decrease in k_{obs}. For ACT, the maximum k_{obs} of 0.02 min^{-1} was observed at pH 8.5, and when pH decreased or increased from 8.5, a reduction in k_{obs} was observed. ATL degradation also showed similar trend with pH variation. Similar findings were reported from previous studies (Wang et al. 2019; Tammaro et al. 2017).

Table 2 Degradation rate constants of ATL and ACT

	ATL			ACT		
Contaminant concentration (mg/L)	5	10	20	5	10	20
R^2 value	0.95	0.94	0.94	0.96	0.96	0.95
Rate constant (k_{obs}) (min^{-1})	0.01	0.009	0.008	0.02	0.012	0.009
% removal	70.2	65.1	58.6	90.8	80.2	70.1

Effect of type of catalyst and catalyst concentration

The performance of ZnO and Ag-ZnO in the degradation of ATL and ACT was evaluated (Fig. 11). The results show an increase in photodegradation efficiency of Ag-ZnO towards ATL and ACT in comparison to ZnO. Photocatalytic efficiency of Ag-ZnO is dictated by crystal structure, particle size distribution, surface area, and bandgap energy. These results indicate that addition of Ag enhances the visible light absorption capacity of ZnO. Accordingly, more photons can be absorbed which improves the photocatalytic efficiency.

Also, it was observed that when catalyst dosage was increased gradually from 1g/L to 1.7 g/L, the degradation efficiency declined from 90.8% to 75% in the case of ACT and similar trend was observed with ATL. Escalating the catalyst loading results in an increased number of catalyst active sites which are available for efficient photocatalyst operation, and this phenomenon continues till all catalyst particles are completely irradiated. After this point, increase in catalyst load led to shading of photoreactive surface which retarded the incident light and thereby flattening the conversion rate of pollutant (Hapeshi et al. 2010).

Characterization of photocatalytic degradation experiments

To evaluate the characterization of photocatalytic degradation of ATL and ACT, further experiments were performed to assess the removal through adsorption, photolytic, and photocatalytic processes (Fig. 12). Experimental conditions for all the characteristic experiments considered were the optimum conditions where maximum removal of both contaminants was achieved. This includes initial contaminant concentration of 5 mg/L, pH of 8.5, catalyst dosage of 1 g/L, and reaction time of 120 min. Adsorption removal was found to be about 4.8% and 3.9% for ATL and ACT, respectively. Experiments performed to evaluate the photolytic removal of contaminants in the presence of a visible light source without the addition of photocatalyst Ag-ZnO resulted in 15.1% removal of ATL and 13% removal of ACT. Lesser adsorption and photolytic removal of ATL and ACT indicate that Ag-ZnO plays a key role as a photocatalyst (in the visible region) for the removal of contaminants. Earlier studies indicate that the removal of pharmaceutical contaminants is dominated by the OH• oxidation pathway rather than by photolysis (Liu et al. 2018; Cheshme Khavar et al. 2019). Removal through OH• generation pathway can be confirmed by employing a nonaqueous solvent like acetonitrile, which eliminates OH• generation in the reaction mechanism. Results of photocatalytic experiments employing acetonitrile as solvent show that ATL and ACT removal was negligible. This indicates that the OH• pathway could play a key role in the removal process. Photocatalytic removal in water medium was found to be 70.2% and 90.8% for ATL and ACT, respectively, confirming that photocatalysis through OH• pathway is the major removal process for eliminating ATL and ACT.

The schematic of possible photocatalytic degradation mechanism of ATL and ACT is shown in Fig. 13.

To study the extent of mineralization of ATL and ACT under the photocatalytic process, TOC and COD were

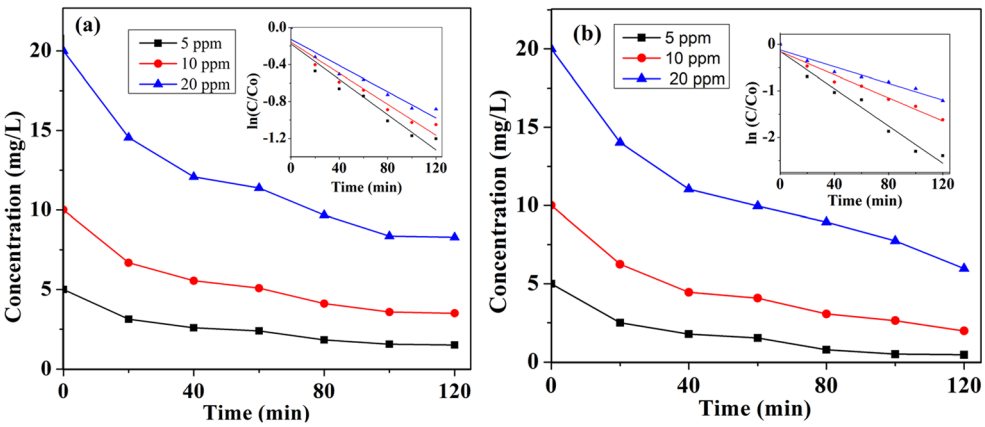

Fig. 9 Effect of initial ATL (**a**) and ACT (**b**) concentration on the degradation efficiency of ATL and ACT (experimental condition: Ag-ZnO: 1 g/L; pH: 8.5)

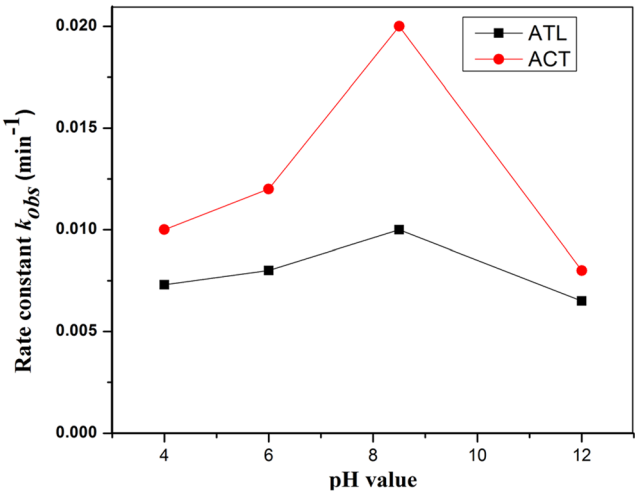

Fig. 10 Effect of pH on the degradation efficiency of ATL and ACT (experimental conditions: $[ATL]_{int}$ = $[ACT]_{int}$ = 5 mg/L and Ag-ZnO= 1 g/L)

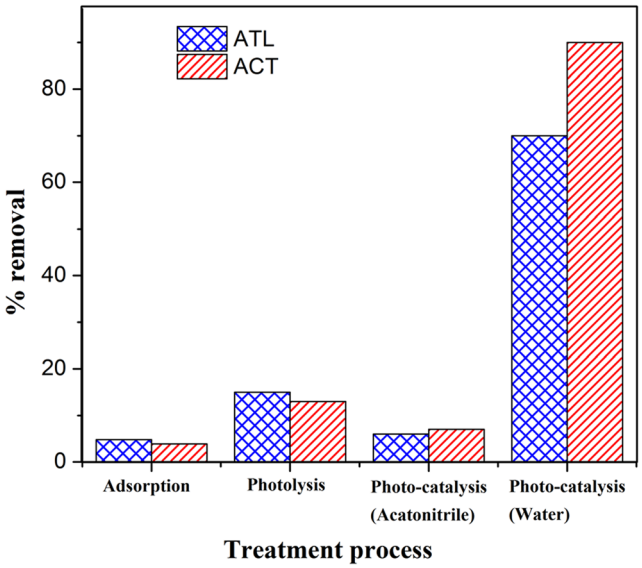

Fig. 12 ATL and ACT removal under different processes (experimental conditions: $[ATL]_{int}$ and $[ACT]_{int}$: 5 mg/L, pH: 8.5, time: 120 min, and Ag-ZnO: 1 g/L)

measured for the treated samples. For ATL, the drop in COD and TOC was about 66.7% and 61.1%, respectively, for a reaction time of 120 min. For ACT, the drop was about 84.6% and 80.3% for COD and TOC, respectively, towards the end of reaction time (120 min). ATL was found to be more recalcitrant than ACT under photocatalytic removal although more than 50% mineralization could be achieved for both the contaminants. Earlier study by Thi and Lee (2017) on ACT degradation using La-doped ZnO reported 85% of TOC reduction in a reaction time of 180 min. Earlier studies on ATL have reported 70% removal of TOC in a reaction period of 180 min (Tammaro et al. 2017; Ponkshe and Thakur 2019).

Reusability of photocatalyst

Separate set of experiments under optimum conditions was performed to evaluate the recyclability of Ag-ZnO photocatalyst for the removal of ATL and ACT. The results are presented in Fig. 14. Ag-ZnO photocatalyst was recovered by filtration and centrifuge processes after each photocatalytic experiment cycle. The recovered Ag-ZnO was employed repetitively as photocatalyst in the subsequent runs. The photocatalytic removal efficiency of ACT reduced from 90.8% to

Fig. 11 Effect of type of photocatalyst on the degradation efficiency of ATL and ACT (experimental condition: $[ATL]_{int}$ = $[ACT]_{int}$ = 5 mg/L, Ag-ZnO= 1 g/L, and pH = 8.5)

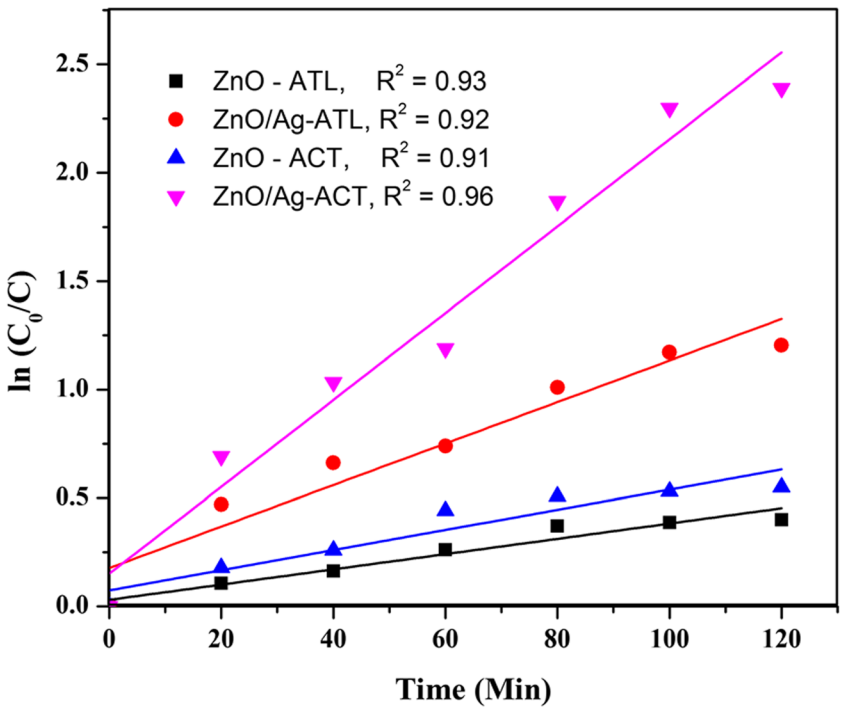

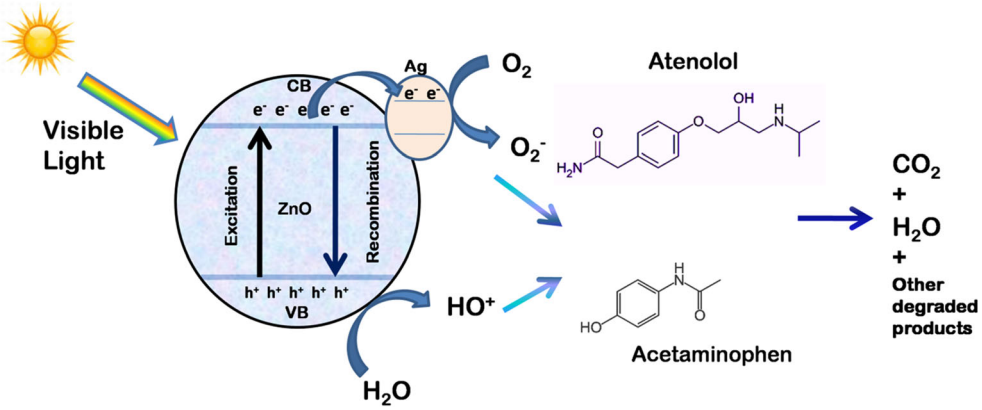

Fig. 13 Schematic diagram of photocatalytic degradation mechanisms of ATL and ACT

76%, whereas for ATL, the reduction was from 70.2% to 59.8% after 5 cycles. The results confirm that Ag-ZnO could be successfully employed for the removal of pharmaceutical contaminants ATL and ACT in wastewater samples.

Conclusion

Ag-ZnO photocatalyst was synthesized using organic approach and employed for the photocatalytic degradation of pharmaceutical residues of ATL and ACT in domestic wastewater effluent. The photocatalyst was characterized using XRD, FTIR, SEM-EDAX, surface area analyzer, UV-visible, and photoluminescence spectrophotometer. From optical studies, it was observed that the absorption edge of Ag-ZnO shifted more towards visible light region in comparison to ZnO. With Ag loading on ZnO, photocatalytic efficiency of ZnO was enhanced and rate constant four times higher than that of bare ZnO was recorded. The photocatalytic degradation of ATL and ACT represented well with pseudo-first-order kinetic model. More prominently, under optimal conditions of 5 mg/L of [ATL] and [ACT], pH of 8.5, catalyst dose of 1 g/L, and reaction time of 120 min, the Ag-ZnO showed the photocatalytic efficiency of 70.2% and 90.8% along with a TOC reduction of 61.1% and 80.3% for ATL and ACT, respectively. The improvement in the efficiency was due to increase in surface area, enhanced charge transfer between ZnO and Ag, and their synergistic effect. Further experiments on photocatalytic mechanism indicate that OH• pathway was the major removal process for eliminating ATL and ACT. Ag-ZnO photocatalyst showed good recycling performance up to 75% removal efficiency after 5 cycles. These findings indicate that the synthesized Ag-ZnO photocatalyst is efficient under visible light radiation and can be practically employed for removing pharmaceutical contaminants.

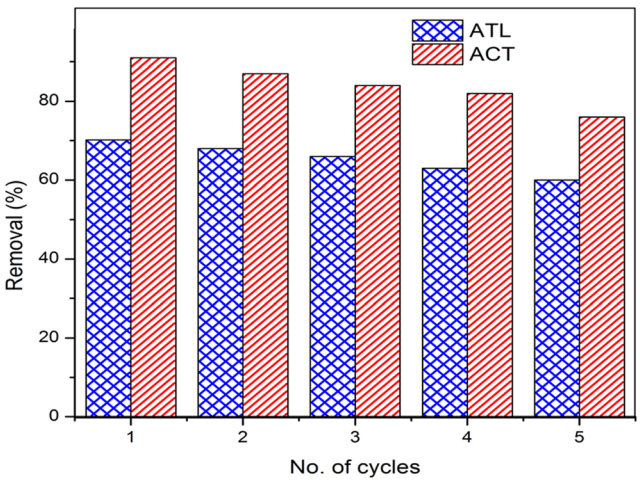

Fig. 14 Effect of recycle times of Ag-ZnO on the photocatalytic removal of pharmaceutical contaminants ATL and ACT

Supplementary Information The online version contains supplementary material available at https://doi.org/10.1007/s11356-021-13532-2.

Author contribution All authors contributed to the study conception and design. Material preparation, experiments, and data collection were performed by Bhuvaneswari R. Data analysis and discussion were performed by Bhuvaneswari R and Dr. C. Prakash. Supervision and validation were done by Dr. J. Jeyanthi. The first draft of the manuscript was written by Bhuvaneswari R, and all authors have subsequently contributed for the improvement of the manuscript. All authors read and approved the final manuscript.

Funding This research work was supported by the Centre of Excellence–Environmental Studies, Government College of Technology, Coimbatore, Tamil Nadu, India.

Data availability All data generated or analyzed during this study are included in this article and its supplementary information files.

Declarations

Ethics approval and consent to participate Not applicable

Consent for publication Not applicable

Competing interests The authors declare no competing interests.

References

Achermann M (2010) Exciton−plasmon interactions in metal−semiconductor nanostructures. J Phys Chem Lett *1*(19):2837–2843. https://doi.org/10.1021/jz101102e

Akir S, Hamdi A, Addad A, Coffinier Y, Boukherroub R, Dakhlaoui Omrani A (2017) Facile synthesis of carbon-ZnO nanocomposite with enhanced visible light photocatalytic performance. Appl Surf Sci 400:461–470. https://doi.org/10.1016/j.apsusc.2016.12.212

Ali K, Dwivedi S, Azam A, Saquib Q, Al-said MS, Alkhedhairy AA et al (2016) Aloe vera extract functionalized zinc oxide nanoparticles as nanoantibiotics against multi-drug resistant clinical bacterial isolates. J Colloid Interface Sci 472:145–156. https://doi.org/10.1016/j.jcis.2016.03.021

Ankush, Mandal MK, Sharma M, Khushboo, Pandey S, Dubey KK (2018) Membrane technologies for the treatment of pharmaceutical industry wastewater. Energy Environ Sustain:103–116. https://doi.org/10.1007/978-981-13-3259-3_6

Aus der Beek T, Weber F, Bergmann A, Hickmann S, Ebert I, Hein A, Küster A (2016) Pharmaceuticals in the environment-global occurrences and perspectives. Environ Toxicol Chem *35*(4):823–835. https://doi.org/10.1002/etc.3339

Balakrishna K, Rath A, Praveenkumarreddy Y, Guruge KS, Subedi B (2017) A review of the occurrence of pharmaceuticals and personal care products in Indian water bodies. Ecotoxicol Environ Saf 137:113–120. https://doi.org/10.1016/j.ecoenv.2016.11.014

Cheshme Khavar AH, Moussavi G, Mahjoub AR, Luque R, Rodríguez-Padrón D, Sattari M (2019) Enhanced visible light photocatalytic degradation of acetaminophen with ag2s-zno@rgo core-shell microsphere as a novel catalyst: catalyst preparation and characterization and mechanistic catalytic experiments. Sep Purif Technol 229:115803. https://doi.org/10.1016/j.seppur.2019.115803

Chinnaiyan P, Thampi SG, Kumar M, Mini KM (2018) Pharmaceutical products as emerging contaminant in water: relevance for developing nations and identification of critical compounds for Indian environment. Environ Monit Assess 190(5):288. https://doi.org/10.1007/s10661-018-6672-9

Chinnaiyan P, Thampi SG, Kumar M, Balachandran M (2019) Photocatalytic treatment of amiodarone and levetiracetam in pharmaceutical industry effluent: process optimization using response surface methodology. Desalin Water Treat 170:253–264. https://doi.org/10.5004/dwt.2019.24727

Elumalai K, Velmurugan S (2015) Green synthesis, characterization and antimicrobial activities of zinc oxide nanoparticles from the leaf extract of Azadirachta indica. Appl Surf Sci 345:329–336. https://doi.org/10.1016/j.apsusc.2015.03.176

Freitas AM, Rivas G, Campos-Mañas MC, Casas López JL, Agüera A, Pérez JAS (2017) Ecotoxicity evaluation of a WWTP effluent treated by solar photo-Fenton at neutral pH in a raceway pond reactor. Environ Sci Pollut Res 24:1093–1104. https://doi.org/10.1007/s11356-016-7101-7

Grenni P, Ancona V, Barra Caracciolo A (2018) Ecological effects of antibiotics on natural ecosystems: a review. Microchem J 136:25–39. https://doi.org/10.1016/j.microc.2017.02.006

Hapeshi E, Achilleos A, Vasquez M, Michael C, Xekoukoulotakis N, Mantzavinos D, Kassinos D (2010) Drugs degrading photocatalytically: kinetics and mechanisms of ofloxacin and atenolol removal on Titania suspensions. Water Res 44(6):1737–1746. https://doi.org/10.1016/j.watres.2009.11.044

Kadam A, Bhopate D, Kondalkar V, Majhi S, Bathula C, Tran A, Lee S (2018) Facile synthesis of Ag-ZnO core–shell nanostructures with enhanced photocatalytic activity. J Ind Eng Chem *61*:78–86. https://doi.org/10.1016/j.jiec.2017.12.003

Kaur A, Gupta G, Alex OI, Deepak BS, Sinha ASK, Sushil KK (2018) A Facile synthesis of silver modified ZnO nanoplates for efficient removal of ofloxacin drug in aqueous phase under solar irradiation. J Environ Chem Eng 6(3):3621–3630. https://doi.org/10.1016/j.jece.2017.05.032

Kavithaa K, Paulpandi M, Ponraj T, Murugan K, Sumathi S (2016) Induction of in- trinsic apoptotic pathway in human breast cancer (MCF-7) cells through facile biosynthesized zinc oxide nanorods. Karbala Int J Mod Sci 2:46–55. https://doi.org/10.1016/j.kijoms.2016.01.002

Khan HK, Rehman MY, Malik RN (2020) Fate and toxicity of pharmaceuticals in water environment: an insight on their occurrence in South Asia. J Environ Manag 271:111030. https://doi.org/10.1016/j.jenvman.2020.111030

Larsson DG (2014) Pollution from drug manufacturing: review and perspectives. Phil Trans R Soc B Biol Sci 369(1656):20130571. https://doi.org/10.1098/rstb.2013.0571

Liu Y, Zhang Q, Xu M, Yuan H, Chen Y, Zhang J, Luo K, Zhang J, You B (2018) Novel and efficient synthesis of Ag-ZnO nanoparticles for the sunlight-induced photocatalytic degradation. Appl Surf Sci 476(September):632–640. https://doi.org/10.1016/j.apsusc.2019.01.137

Mohd AMA, Nurhidayatullaili MJ, Sharifah BAH (2016) Review on ZnO hybrid photocatalyst: impact on photocatalytic activities of water pollutant degradation. Rev Inorg Chem 36(2). https://doi.org/10.1515/revic-2015-0015

Moles S, Valero P, Escuadra S, Mosteo R, Gómez J, Ormad MP (2020) Performance comparison of commercial TiO2: separation and reuse for bacterial photo-inactivation and emerging pollutants photo-degradation. Environ Sci Pollut Res 27:9099–9113. https://doi.org/10.1007/s11356-019-07276-3

Patel M, Kumar R, Kishor K, Mlsna T, Pittman CU, Mohan D (2019) Pharmaceuticals of emerging concern in aquatic systems: chemistry, occurrence, effects, and removal methods. Chem Rev 119(6):3510–3673. https://doi.org/10.1021/acs.chemrev.8b00299

Ponkshe A, Thakur P (2019) Significant mineralization of beta blockers propranolol and Atenolol by TiO2 induced photocatalysis. Mater Today Proc 18:1162–1175. https://doi.org/10.1016/j.matpr.2019.06.577

Sajan CP, Naik A, Girish HN, Ravi HR, Singh R (2017) Template-free processing of Ag-anchored ZnO polyscale sheets and their application in the photocatalytic degradation of organics present in pharmaceutical waste. Water Conserv Sci Eng 2(2):31–41. https://doi.org/10.1007/s41101-017-0022-6

Schröder P, Helmreich B, Škrbić B, Carballa M, Papa M, Pastore C, Emre Z, Oehmen A, Langenhoff A, Molinos M, Dvarioniene J, Huber C, Tsagarakis KP, Martinez-Lopez E, Pagano SM, Vogelsang C, Mascolo G (2016) Status of hormones and painkillers in wastewater effluents across several European states—considerations for the EU watch list concerning estradiols and diclofenac. Environ Sci Pollut Res 23:12835–12866. https://doi.org/10.1007/s11356-016-6503-x

Sundrarajan M, Ambika S, Bharathi K (2015) Plant-extract mediated synthesis of ZnO nanoparticles using Pongamia pinnata and their activity against pathogenic bacteria. Adv Powder Technol 26:1294–1299. https://doi.org/10.1016/j.apt.2015.07.001

Sushma C, Girish Kumar S (2017) Advancements in the zinc oxide nanomaterials for efficient photocatalysis. Chem Pap 71(10):2023–2042. https://doi.org/10.1007/s11696-017-0217-5

Tammaro M, Fiandra V, Mascolo MC, Salluzzo A, Riccio C, Lancia A (2017) Photocatalytic degradation of atenolol in aqueous suspension of new recyclable catalysts based on titanium dioxide. J Environ Chem Eng 5(4):3224–3234. https://doi.org/10.1016/j.jece.2017.06.026

Thi VH, Lee B (2017) Effective photocatalytic degradation of paracetamol using la-doped ZnO photocatalyst under visible light irradiation. Mater Res Bull 96:171–182. https://doi.org/10.1016/j.materresbull.2017.04.028

Tran NH, Reinhard M, Gin KYH (2018) Occurrence and fate of emerging contaminants in municipal wastewater treatment plants from different geographical regions-a review. Water Res 133(December):182–207. https://doi.org/10.1016/j.watres.2017.12.029

Wang S, Wu J, Lu X, Xu W, Gong Q, Ding J, Dan B, Xie P (2019) Removal of acetaminophen in the Fe2+/persulfate system: kinetic model and degradation pathways. Chem Eng J 358:1091–1100. https://doi.org/10.1016/j.cej.2018.09.145

Yadav KK, Kumar A, Kumar A, Misra N, Brahmachari G (2018) Structure, spectroscopic analyses (FT-IR and NMR), vibrational study, chemical reactivity and molecular docking study on 3,3'-((4-(trifluoromethyl)phenyl)methylene)bis(2-hydroxynaphthalene-1,4-dione), a promising anticancerous bis-lawsone derivative. J Mol Struct 1154:596–605. https://doi.org/10.1016/j.molstruc.2017.09.095

Zare M, Namratha K, Alghamdi S, Mohammad YH, Hezam A, Zare M, Drmosh QA, Byrappa K, Chandrashekar BN, Ramakrishna S, Zhang X (2019) Novel green biomimetic approach for synthesis of ZnO-Ag nanocomposite; antimicrobial activity against food-borne pathogen, biocompatibility and solar photocatalysis. Sci Rep 9(1):8303. https://doi.org/10.1038/s41598-019-44309-w

Zulkifli F, Ali N'a, Yusof MSM, Khairul WM, Rahamathullah R, Isa MIN, Nik WBW (2017) The effect of concentration of Lawsonia inermis as a corrosion inhibitor for aluminum alloy in seawater. Adv Phys Chem. https://doi.org/10.1155/2017/8521623